Universal Journal of Green Chemistry
https://ojs.wiserpub.com/index.php/UJGC/

Research Article

A Green Route for Sustainable Nanoporous Solid Acid Catalyst Synthesis Using Bio Template and Analysis of Its Progressive Transformation of CO_2

M.A. Mary Thangam*, Chellapandian Kannan

Department of Chemistry, Manonmaniam Sundaranar University College, Govindaperi, Tirunelveli 627414, Tamilnadu, India
E-mail: marythangam2010@gmail.com

Received: 21 November 2023; **Revised:** 3 January 2024; **Accepted:** 4 February 2024

Abstract: Green chemistry approach is a most important area in the modern chemical world. The nano (meso) porous materials have the specific application in separation, adsorption and catalysis. A green template (Egg white) is used as a bio template for the synthesis of nanoporous material to replace the hazardous templates. It is a bio-degradable template; it does not create any environmental issues. The synthesized material is characterized by various spectroscopic techniques to confirm its structural formation. Based on pore size, the catalyst named as $AlSiO_4$-14. The synthesized catalyst ($AlSiO_4$-14) is active at 175 °C. This low temperature activity will not produce coke formation at the same time it does not require any regeneration and the catalyst is continuously active for catalytic reactions. The catalytic activity of carbon dioxide decomposition is achieved at lower temperature. The complete carbon dioxide decomposition of $AlSiO_4$-14 is 43% is a great impact of the material.

Keywords: porous material; green template; $AlSiO_4$-14; complete decomposition; Eco-friendly

1. Introduction

Nanoporous solid acid catalysts are the most interesting materials for the enormous uses in various fields such as adsorption, petro chemical industries, catalysis, catalytic supports, sensors and fuel cells [1–7]. The mesoporous framework containing materials has the pore size between 2 nm to 50 nm [2,4]. The porous framework materials are used to separate different types of molecules from a mixture of molecules. The majority of the porous solid acid materials had the greatest impact on green chemistry applications, however the molecular sieves synthesize method is not under the green chemistry. Most of the conventional templates are used for the synthesis is not eco friendly. In this present work, we have synthesized the nanoporous aluminosilicate molecular sieves using bio template it does not create any corrosion and pollution to the environment. It is an inexpensive template compared to the conventional templates. Conventional templates like tetraethylammonium hydroxide (TEAOH) [8], organic amines [9,10], hexamethyleneimine [11,12], alkyltrimethylammoniam halides (C*n*TMAX; X) Cl or Br) [9,13], geminisurfactants type ($[C_nH_{2n+1}N^+(CH_3)_2(CH_2)sN^+\text{-}(CH_3)_2C_mH_{2m+1}]Br_2$)(18-12-18) [14], Myristyltrimethylammonium bromide (MTMAB) [15], dodecyltrimethylammonium bromide [13], diblock copolymer, triblock copolymer P123 (nonionic surfactant) [4,16,17], oligomeric surfactants [4], Rhodamine B (dye) [3], ω-hydroxy-bolaform surfactants [18] fatty alcohol polyoxyethylene ether (PEO surfactants) [19] are used as a template. In a few synthesis methods NaOH [19], butanol [15] and carbon black microspheres [11] is used as a co-surfactant. Cetyltrimethyl ammonium bromide

DOI: https://doi.org/10.37256/ujgc.2120244388

(CTABr) [16,20,21] is a most common structure directing agent for synthesizing a mesoporus molecular sieves. These structure directing agents are chemically harmful. The synthesized nanoporous materials are mainly used for green chemistry applications, but the synthesizing method is not a green process. To overcome these obstacles, egg white is used as a template (green template).

2. Experimental Section

2.1 *Green-Template*

Egg white is used as a bio-template for the synthesis of $AlSiO_4$ material. Egg white is mainly made-up by water and protein. 55% of the egg white is made up of Albumin and remaining proteins are transferring, mucoid, globulin G2, globulin G3, mucin and lysozyme. To avoid hazardous templates, egg white is used as a green and bio-template. $AlSiO_4$ material is synthesized from inexpensive source material & simple method using green template.

2.2 *Materials and Methods*

$AlCl_3$ (98% Merck), Na_2SiO_3 (meta) (Loba Chemie) and Egg white is used as a template.

In a distinctive synthesis, 13.5 g (0.0135 mmole) of aluminium chloride is suspended in aqueous medium with constant stirring. After that, 28.5 g (0.0285 mmole) of sodium silicate fine particles is included and 25 mL of egg white is mixed with it. Further the reactants is stirred continuously for 30 min and kept aside for 24 h to achieve the product. The obtained material is continuously cleaned with distilled water as well as dehydrated at 120 °C for 2 h.

2.3 *Calcination*

To remove the unwanted volatile compounds and templates from the aperture of the as-prepared material, it is calcinated at 600 °C with the help of air. During the calcinations, the white material turns into brown and this is due to the fragmentation of template. This indicated that some organic volatile fragments are present inside the pores of the catalyst. After the complete removal of template, the material became white powder.

2.4 *Catalytic Reactor Set Up*

In CO_2 decomposition, curved catalytic reactor is developed. Transformation of carbon dioxide continuously analyzed by the reactor (Figure 1). The reactor is packed with calcinated material and it is kept under engine oil. The reactor is heated in a hot plate and the temperature is monitored by thermometer. 99.6% of unpolluted carbon dioxide is passed through the inlet and the outlet is sealed by stopcocks.

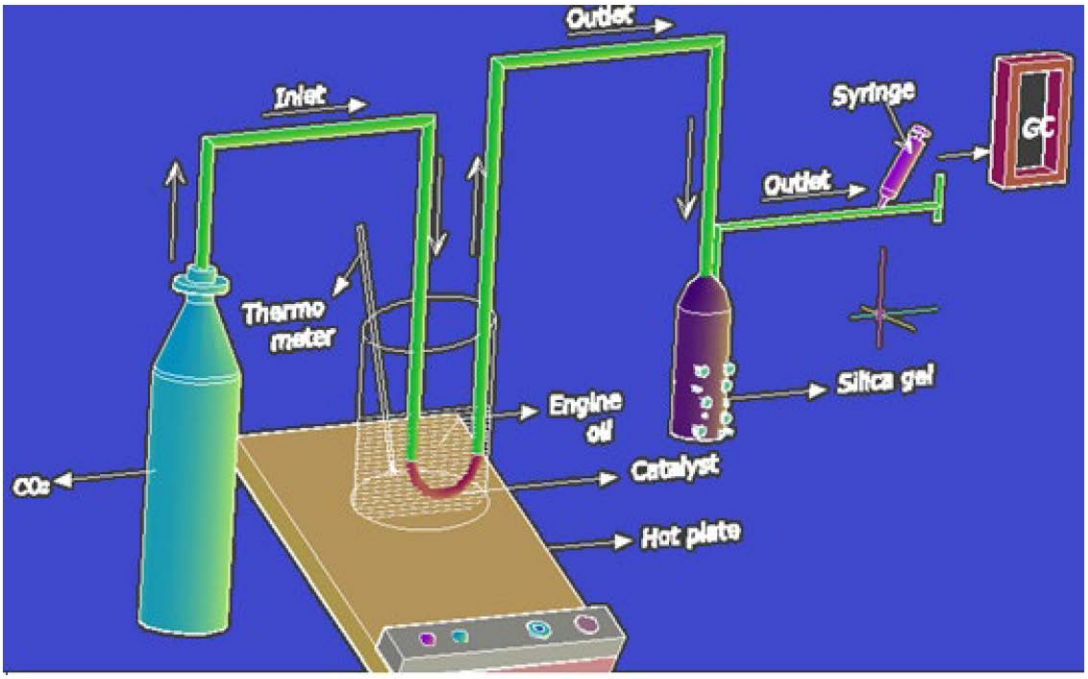

Figure 1. Curved CO_2 catalytic reactor.

2.5 *Regeneration & Reusability of the Catalyst*

For regenerating the catalyst, the catalysts are taken in a U-shape tube with inlet and outlet containing tube, this tube is fitted in a sigma electric Bunsen and it is heated for a high temperature (above 400 °C). Air is generated from aerator and it is passed though KOH solution for removing the CO_2 and it is connected with silica gel (blue) for removing moisture. The CO_2 and H_2O free air is passed to the catalytic bed for regeneration.

2.6 *Characterization Techniques*

The structural formation and crystallinity of the material is analyzed on Bruker D8 advance Low-angle X-Ray Diffraction (XRD) (Cu-α radiation, λ = 1.5418Å). Symmetric and asymmetric stretching is recorded by JASCO-410FT-IR (KBr pellet method). Chemisoft TPx V1.02 is used to record the TPD (NH_3 desorption). Removal of template from the material is recorded from TGA Q500 V20.10. Micrometrics, ASAP 2020 V3.00H is used to evidence the porous nature of the material. The morphology and elements of the material is analyzed with a help of Scanning Electron Micrograph (SEM) of Carl Zeiss EVO 18. Carbon dioxide decomposition products are analyzed with Gas Chromatography (Thermo Fischer/chemito GC 1000) using TCD.

3. Results and Discussion

3.1 *Small Angle X-Ray Diffraction*

The synthesized material is calcinated at 450 °C for the complete elimination of all the templates from the cavities of the material. The XRD pattern (Figure 2) shown that, the material is thermally stable and crystalline. The formation of nanoporous (meso) [1,4] is confirmed by the intense small angle peak at 1.1 degree and it is in 100 and 110 plane. This XRD analysis proved that the egg white acting as a template for the formation of nanopores in this material.

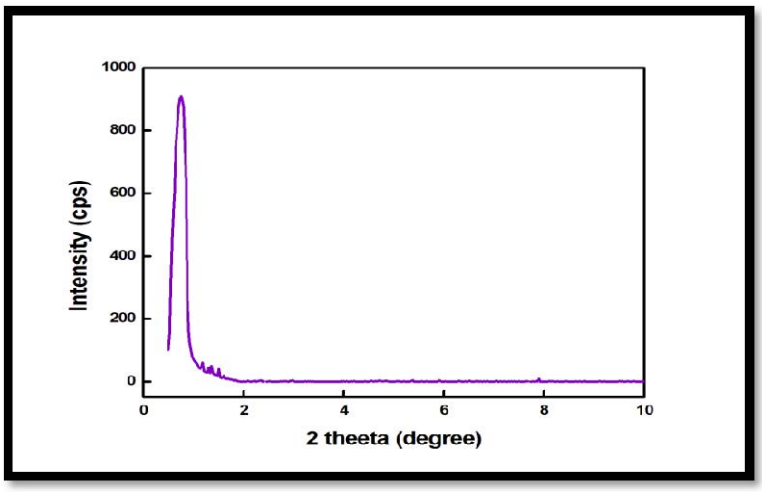

Figure 2. XRD pattern of calcinated bio-templated $AlSiO_4$.

3.2 *FT-IR Analysis*

The broad peaks from 3700 to 3000 cm^{-1} in the as-prepared material is owing to the occurrence of water molecule and the C-H stretching vibrations between 2000 to 1600 cm^{-1} is caused by the incidence of template in the cavities after calcination these peaks get disappeared (Figure 3)[22]. The material shows the fundamental vibrations of symmetric stretching and bending vibrations at 790, 430 cm^{-1} respectively. The distinctive peak at 1086 cm^{-1} proves the formation of tetrahedral frame work[23–26]. This spectrum confirms that the tetrahedral frame work is stable after calcination at higher temperature.

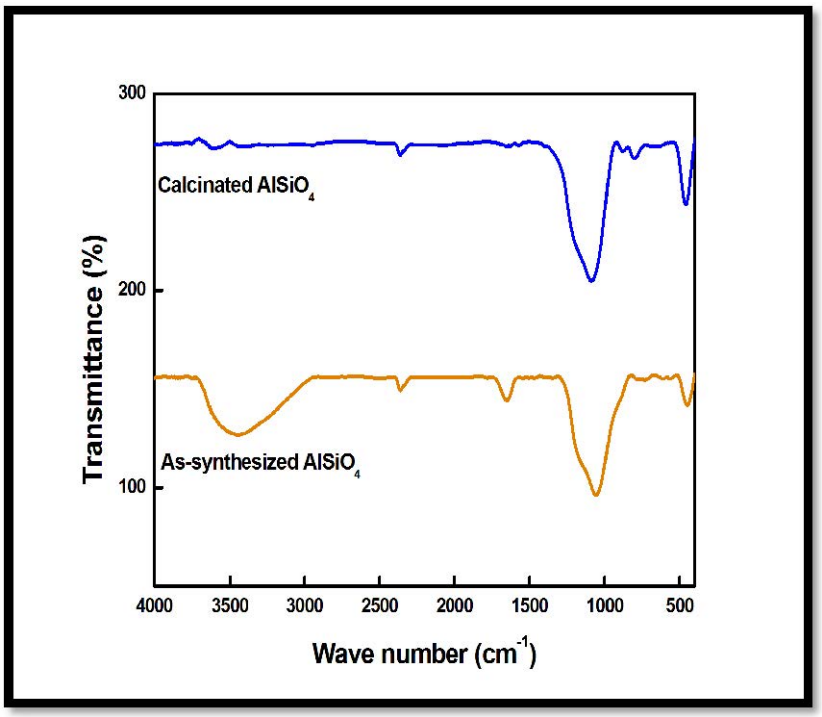

Figure 3. FT-IR spectrum of as-synthesized & calcinated $AlSiO_4$ (bio-templated).

3.3 *Thermal Analysis*

From thermogravimetry (Figure 4), the weight change is observed from 50 °C to 950 °C. The first weight loss observed from 100 °C to 220 °C, it is due to the elimination of reactive and non-reactive water molecules from the outer layer and pores of the catalyst evidenced by endothermic peaks of DTA curves[24,25]. The second weight loss arises at 500 °C due to entire elimination of bio-template from the cavities with evidence of exothermic peak[27,28]. The final weight loss at 910 °C may be due to the adjacent OH group condensation[27]. TGA curve of $AlSiO_4$ material shows, it is highly thermally stable up to 950 °C.

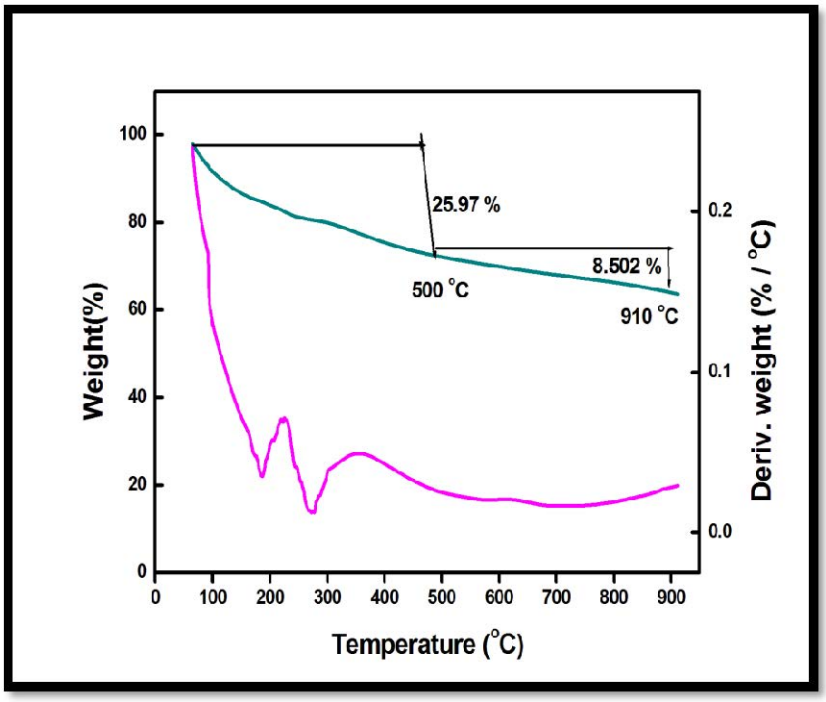

Figure 4. TGA curve for as-synthesized $AlSiO_4$ (bio-templated).

3.4 *TPD Analysis*

Acidic character of the calcinated material is analyzed from NH_3 Temperature Programmed Desorption (Figure 5). The material has 0.2091 mmole/g of acidity. The catalyst is active at 175 °C and above. The synthesized material has a series of acid sites from weak, moderate and strong[28,29].

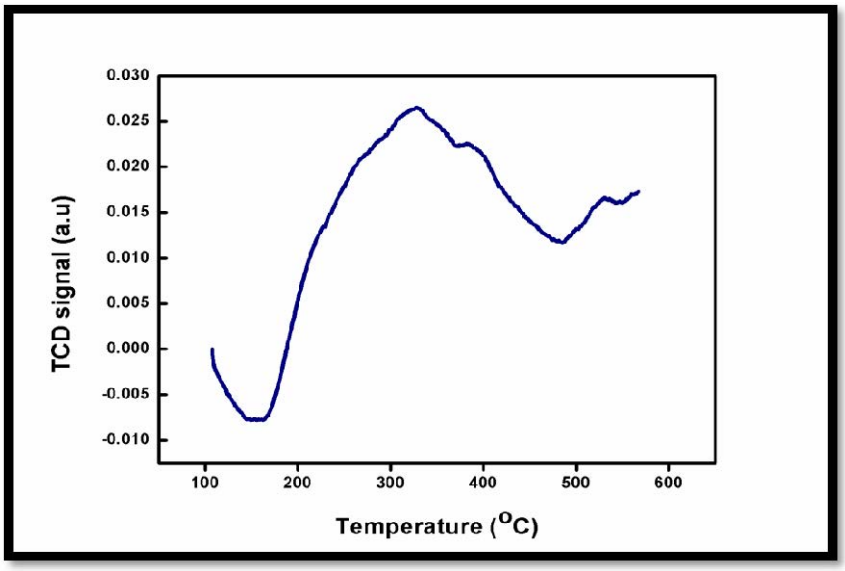

Figure 5. NH_3 TPD for calcinated bio-templated $AlSiO_4$.

3.5 *N_2 Adsorption Isotherm*

From Figure 6, the surface area of the calcinated substanceis 42.3077 m^2/g and its pore size is 14 nm. Type IV isotherm hysteresis loop from 0.1–0.9 (p/p_0) belongs to the adsorption of N_2 in nanoporous walls. From the above result, it is confirmed the formation of mesoporous material[30,31]. **The pore size of the material is 14 nm. Hence it is named as $AlSiO_4$–14.** A Physico-chemical property of the $AlSiO_4$–14 material is tabulated in Table 1.

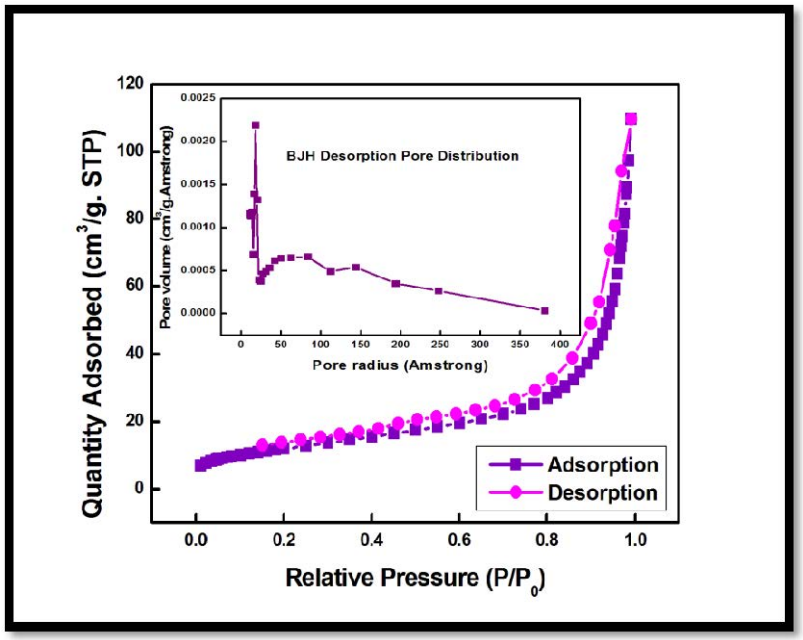

Figure 6. N_2 Adsorption isotherm of calcinated $AlSiO_4$–14.

Table 1. Physico-chemical properties of $AlSiO_4$-14.

Catalyst	Total Acid (mmol/g)	S_{BET} (m^2/g)	Pore Size (nm)	V_{meso} (cm^3/g)
$AlSiO_4$-14	0.20	42.3	14.1	0.17

3.6 *SEM and EDX Analysis*

Photographical views of the thermally treated $AlSiO_4$-14 are verified from SEM analysis (Figure 7). SEM analyses give the feature about the particle dimension and contour of the outer face of the material[32]. Type of porosity, pore annulled and particle agglomerations are studied. Moreover the pores are observable and pores are ordered particle sizes are disordered.

The amount of Al-O-Si in the synthesized material is analyzed by elemental analysis. The selected area of EDX investigation proves the occurrence of distinctive peak of $AlSiO_4$ in Figure 8 and the molar composition is 1:4:1 (Al: 4O: Si). From this outcome, it is confirmed that the material is in tetrahedral framework.

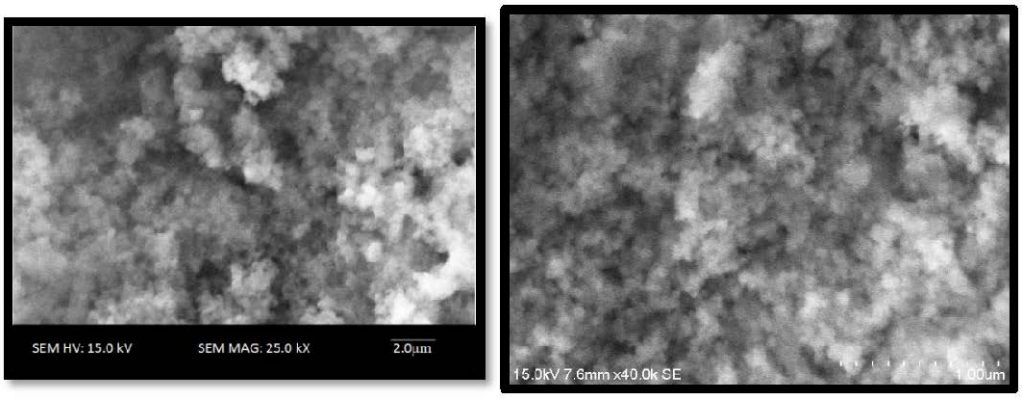

Figure 7. SEM images of calcinated $AlSiO_4$-14.

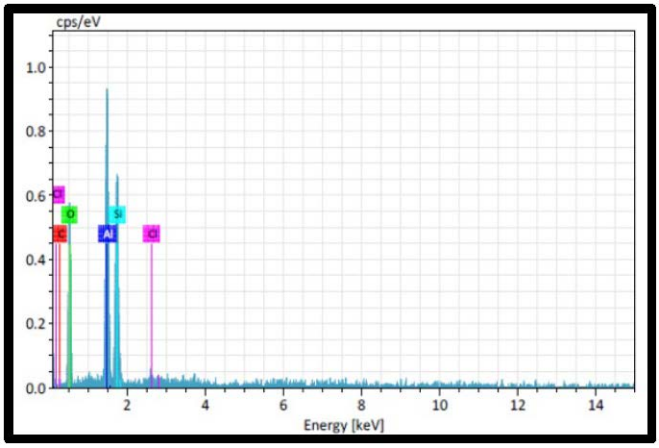

Figure 8. EDX spectrum of calcinated $AlSiO_4$-14.

4. Catalytic Study of Carbon Dioxide Decomposition

The catalyst is applied for carbon dioxide decomposition reaction to evaluate the catalytic activity and the catalytic reactor setup is shown in Scheme 1. Bio-templated $AlSiO_4$–14 decomposes the CO_2 molecules by the following reaction mechanism and it is given below.

During the reaction the $2CO_2$ dissociates as 2CO and O_2. The acidic sites of the catalyst further decompose the carbon monoxide into carbon and oxygen.

$$2CO_2 \xrightarrow{\text{catalytic cracking}} 2CO + O_2 \tag{1}$$

Further the catalytic cracking of CO gives carbon and oxygen.

$$2CO \longrightarrow 2C + O_2 \tag{2}$$

The reaction mechanism is mainly developed by the presence of active acid sites of the material. In acidic material, the CO_2 molecule is decomposed and forms as stable carbon monoxide and release oxygen.

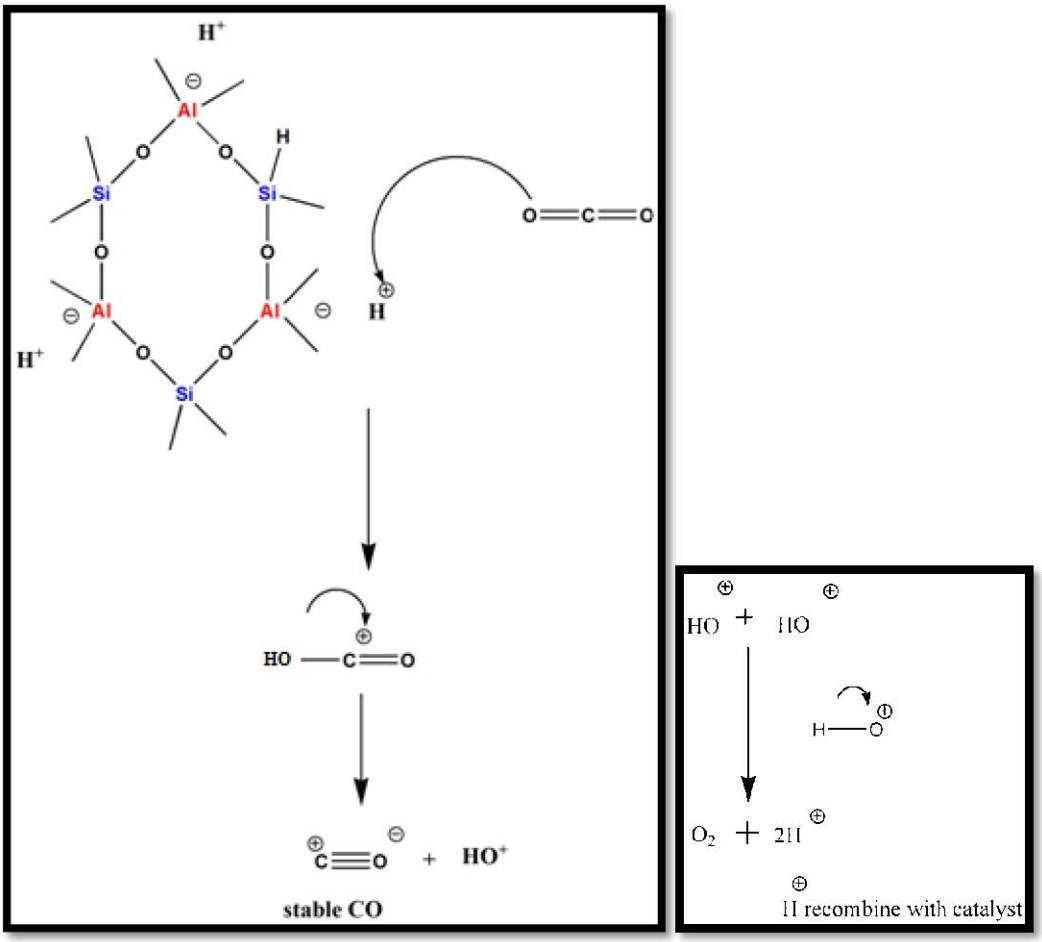

Scheme 1. CO_2 decomposition mechanism of $AlSiO_4$–14.

4.1 *Effect of Temperature*

Decomposition of carbon dioxide has been studied from 60 to 200 °C for $AlSiO_4$-14 and the conversion percentage is tabulated in Table 2 (Figure 9).

Conversion is more at 70 °C and the oxygen product selectivity is poor compared to carbon monoxide. Further increase of temperature, oxygen selectivity increased and carbon monoxide selectivity is decreased. However the carbon dioxide transformation reduces with increase of heat. It is revealed that partial decomposition decreased with increase of temperature or complete decomposition increases with increase of temperature.

Table 2. Result of heat on transformation of CO_2 over $AlSiO_4$-14.

Catalyst	Temperature (°C)	Carbon Dioxide Transformation (%)			Product Conversion (%)	
		Complete Transformation	Partial Transformation	Total Transformation	CO	O_2
$AlSiO_4$-14	60	4	3	7	51	48
	70	**5**	**15**	**20**	**73**	**26**
	80	7	4	11	47	52
	100	10	4	14	51	48
	150	7	1	8	25	74
	200	6	1	7	18	81

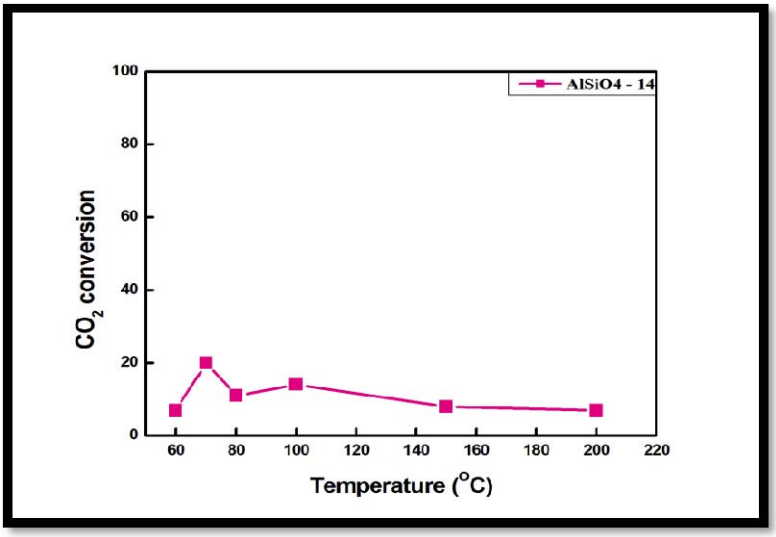

Catalyst dose: 0.5 g; flow rate: 0.5 ml/min; Time: 1 h

Figure 9. Result of heat on transformation of CO_2 over $AlSiO_4$-14.

4.2 *Effect of Flow Speed*

Effect of flow speed started from 0.5 to 2.5 mL per min over $AlSiO_4$-14 is exposed in Figure 10. $AlSiO_4$-14 show highest change of carbon dioxide at 0.5 mL per min, further raise of flow rate, selectivity of carbon monoxide is increased and oxygen decreased. Conversion of carbon dioxide (partial decomposition and complete decomposition) also decreased with increase of flow rate. It may be caused by the diffusion of cavities with carbon dioxide molecules. This study confirms that the most favorable flow speed for $AlSiO_4$-14 is 0.5 mL per min (Table 3).

Table 3. Result of flow rate on transformation of CO_2 over $AlSiO_4$–14.

Catalyst	Flow Rate (mL/min)	Carbon Dioxide Transformation (%)			Product Conversion (%)	
		Complete Transformation	Partial Transformation	Total Conversion	CO	O_2
$AlSiO_4$–14	0.5	5	15	20	73	26
	1.5	3	15	18	86	13
	2.5	2	14	16	90	9

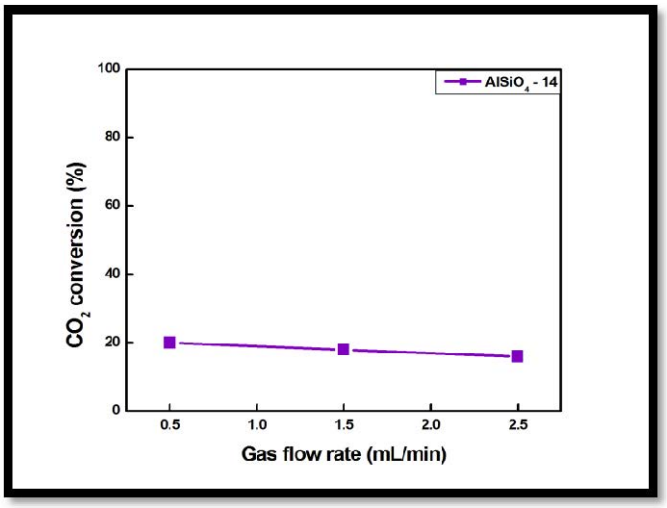

Catalyst dose: 0.5 g; temperature $AlSiO_4$-14 (70°C); Time: 1 h

Figure 10. Result of gas flow rate on transformation of CO_2 over $AlSiO_4$–14.

4.3 *Result of Catalyst Dosage*

Loading of catalyst dosage verified from 0.5 to 2.5 g (Table 4 & Figure 11). Utmost transformation of carbon dioxide is found at 2.5 g over $AlSiO_4$–14. Product selectivity of oxygen is also good with increase of catalyst dosage. $AlSiO_4$–14 does not undergo any recombination process when there is boost of catalyst quantity, the conversion & product selectivity (mainly O_2) is raised and CO selectivity is decreased.

Table 4. Result of catalyst dosage on transformation of CO_2 over $AlSiO_4$–14.

Catalyst	Catalyst Dosage (g)	Carbon Dioxide Transformation (%)			Product Conversion (%)	
		Complete Transformation	Partial Transformation	Total Conversion	CO	O_2
$AlSiO_4$–14	0.5	5	15	20	73	26
	1.5	13	24	37	74	25
	2.5	42	31	73	47	52

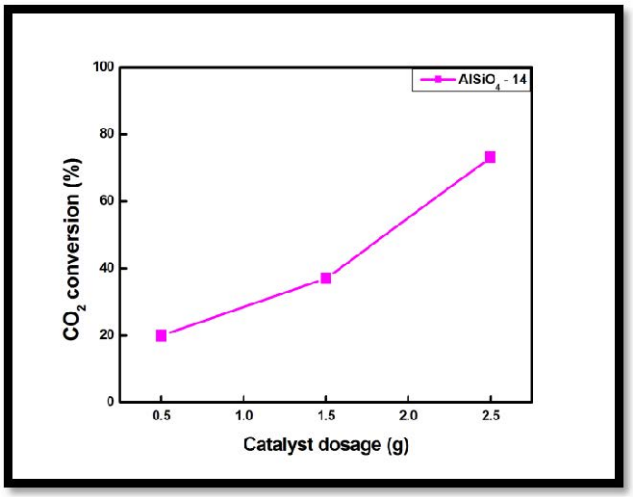

Flow speed: 0.5 ml / min; temperature $AlSiO_4$-14 (70°C); Time: 1 h

Figure 11. Result of catalyst dosage on transformation of CO_2 over $AlSiO_4$- 14.

4.4 *Effect of Time on Flow*

Time on flow has been studied over $AlSiO_4$- 14 catalyst continuously up to 5 h with optimized conditions (Figure 12). The conversion (complete & partial decomposition) of CO_2 and product selectivity of carbon monoxide and oxygen are shown in Table 5. There are no significant changes in CO_2 conversion and product selectivity (CO & O_2). It indicated that the catalyst is active for long time. The carbon may be deposited in the pores. It may also promote the reaction; hence, activity of the catalyst is maintained during the reaction.

Table 5. Effect of time on flow for the decomposition of CO_2 over $AlSiO_4$- 14.

Catalyst	Contact Time (h)	CO_2 Transformation (%)			Product Conversion (%)	
		Complete Transformation	Partial Transformation	Total Conversion	CO	O_2
$AlSiO_4$- 14	1	43	31	74	42	57
	2	51	40	91	44	55
	3	51	40	91	44	55
	4	52	40	92	43	56
	5	48	45	93	48	51

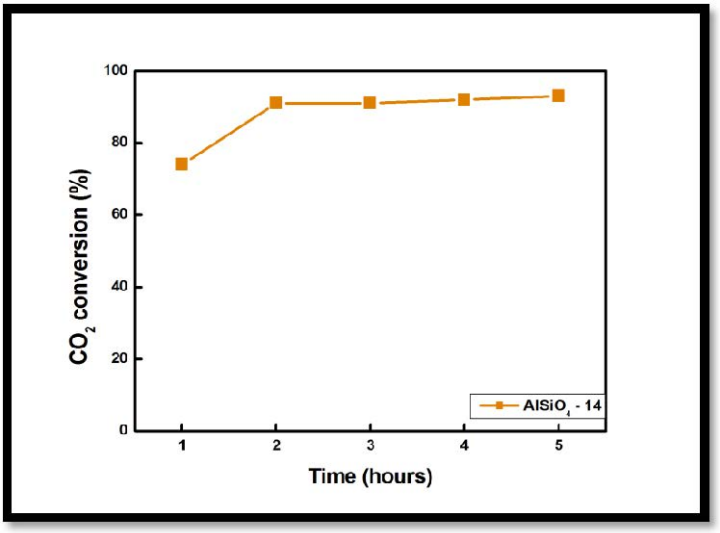

Temperature 70°C; Flow speed: 0.5 mL / min; Catalyst dose: 2.5 g

Figure 12. Result of time on flow for the transformation of CO_2 over $AlSiO_4$–14.

4.5 *Complete Transformation of Carbon Dioxide*

Complete transformation of carbon dioxide is shown in Table 6. $AlSiO_4$–14 decomposed nearly 43 to 50% of carbon dioxide (average 49%) during the time on stream and its partial decomposition average is 39%. The surface area is low and pore size is large. However, the conversion is achieved 49%. It may be due to the nature of template, acidity and cavity size of the catalyst.

Table 6. Complete transformation of carbon dioxide on $AlSiO_4$–14.

Catalyst	Optimized Temperature (°C)	Total Acid (mmol/g)	S_{BET} (m^2/g) Surface Area	Pore Size (nm)	Complete CO_2 Decomposition (%)
$AlSiO_4$–14	70	0.2091	42.3	14.1	43

5. Conclusions

Eco friendly and economically inexpensive bio-material based $AlSiO_4$–14 catalyst is synthesized and characterized. From the analytical studies, the synthesized catalyst has high thermal stability up to 900 °C, surface area is 42.3077 m^2/g and its pore size is 14 nm. From TPD, the synthesized material is active at 175 °C and above, acidity of the material is 0.209 mmol/g. Egg white created the specific features in the material. One of the main advantages of the material is, there is no coke formation during the reaction due to the presence of low temperature active acid sites. Finally its catalytic activity is experienced by carbon dioxide decomposition reaction and various experimental conditions are optimized for maximum conversion and selectivity. Comparing with other material bio-templated $AlSiO_4$–14 produced 75 to 93% of conversion and 70 (CO) & 30 (O_2) percentage of product selectivity. The catalyst can decompose the carbon dioxide molecules constantly. The complete decomposition of CO_2 molecules are achieved 43% by $AlSiO_4$–14 catalyst.

Acknowledgement

I would like to express my sincere thanks to Department of Science and Technology (DST/INSPIRE Fellowship/2015/150040 dated on 1 October 2015) for financial support.

Confilict of Interest

The authors Dr. M.A. Mary Thangam and Dr. C. Kannan have no conflict of interest.

References

[1] Kannan, C.; Sivakami, K.; Jeyamalar, J. I. A simple method for the synthesis of thermally stable large pore mesoporous aluminophosphate molecular sieves. *Mater. Lett.* **2013**, *113*, 93-95. https://doi.org/10.1016/j.matlet.2013.08.129.

[2] Zang, J.; Chempath, S.; Konduri, S.; Nair, S.; Sholl, D. S. Flexibility of Ordered Surface Hydroxyls Influences the Adsorption of Molecules in Single-Walled Aluminosilicate Nanotubes. *J. Phys. Chem. Lett.* **2010**, *1*, 1235-1240. https://doi.org/10.1021/jz100219q.

[3] Mary Thangam, M. A.; Jeyamalar, J. I.; Kannan, C. A New Template for the synthesis of Nanoporous silicate Material. *J. Chem. Pharm. Sci.* **2016**, *9*, 2460-2463.

[4] Wan, Y.; Shi, Y.; Zhao, D. Designed synthesis of mesoporous solids via nonionic-surfactant-templating approach. *Chem. Commun.* **2006**, 897-926. https://doi.org/10.1039/b610570j.

[5] Lin, H. -P.; Wong, S. -T.; Mou, C. -Y.; Tang, C. -Y. Extensive Void Defects in Mesoporous Aluminosilicate MCM-41. *J. Phys. Chem. B.* **2000**, *104*, 8967-8975. https://doi.org/10.1021/jp001569p.

[6] Gora-Marek, K.; Datka, J. IR studies of OH groups in mesoporous aluminosilicates. *Appl. Catal A Gen.* **2006**, *302*, 104-109. https://doi.org/10.1016/j.apcata.2005.12.027.

[7] Yu, C.; Chu, H.; Wan, Y.; Zhao, D. Synthesis of easily shaped ordered mesoporous titanium-containing silica. *J. Mater. Chem.* **2010**, *20*, 4705-4714. https://doi.org/10.1039/b925864g.

[8] Liu, Y.; Pinnavaia, T. J. Aluminosilicate Nanoparticles for Catalytic Hydrocarbon Cracking. *J. Am. Chem. Soc.* **2003**, *125*, 2376-2377. https://doi.org/10.1021/ja029336u.

[9] Sastre, G.; Lewis, D. W.; Richard, C.; Catlow, A. Structure and Stability of Silica Species in SAPO Molecular Sieves. *J. Phys. Chem.* **1996**, *100*, 6722-6730. https://doi.org/10.1021/jp953362f.

[10] Yang, M.; Tian, P.; Liu, L.; Wang, C.; Xu, S.; He Y.; Liu, Z. Cationic surfactant-assisted hydrothermal synthesis: An effective way to tune the crystalline phase and morphology of SAPO molecular sieves. *Cryst. Eng. Comm.* **2015**, *15*, 8555-8561. https://doi.org/10.1039/C5CE01702E.

[11] Chu, N.; Wang, J.; Zhang, Y.; Yang, J.; Lu, J.; Yin, D. Nestlike hollow hierarchical MCM-22 microspheres: Synthesis and exceptional catalytic properties. *Chem. Mater.* **2010**, *22*, 2757-2763. https://doi.org/10.1021/cm903645p.

[12] Ji, Y. -J.; Xu, H.; Wang, D. -R.; Xu, L.; Ji, P.; Wu, H.; Wu, P. Mesoporus MCM-22 zeolites prepared through organic amine-assisted reversible structural change and protective desilication for catalysis of bulky molecules. *ACS Catal.* **2013**, *3*, 1892-1901. https://doi.org/10.1021/cs400284g.

[13] Alam, N.; Mokaya, R. Strongly acidic mesoporous aluminosilicates prepared via hydrothermal restructuring of a crystalline layered silicate. *J. Mater. Chem. A.* **2015**, *3*, 7799-7809. https://doi.org/10.1039/c5ta00548e.

[14] Solberg, S. M.; Kumar, D.; Landry, C. C. Synthesis, Structure, and Reactivity of a New Ti-Containing Microporous/Mesoporous Material. *J. Phys. Chem. B.* **2005**, *109*, 24331-24337. https://doi.org/10.1021/jp054187y.

[15] Kovalchuk, T. V.; Sfihi, H.; Korchev, A. S.; Kovalenko, A. S.; Il'In, V. G.; Zaitsev, V. N.; Fraissard, J. Synthesis, Structure, and Acidic Properties of MCM-41 Functionalized with Phosphate and Titanium Phosphate Groups. *J. Phys. Chem. B.* **2005**, *109*, 13948-13956. https://doi.org/10.1021/jp0580625.

[16] Stevens, W. J. J.; Lebeau, K.; Mertens, M.; Van Tendeloo, G.; Cool, P.; Vansant, E. F. Investigation of the Morphology of the Mesoporous SBA-16 and SBA-15 Materials. *J. Phys. Chem.* **2006**, *110*, 9183-9187. https://doi.org/10.1021/jp0548725.

[17] de Zarate, D. O.; Bouyer, F.; Zschiedrich, H.; Kooyman, P. J.; Trens, P.; Iapichella, J.; Durand, R.; Guillem, C.; Prouzet, E. Micromesoporous Monolithic Al-MSU with a Widely Variable Content of Aluminum Leading to Tunable Acidity. *Chem. Mater.* **2008**, *20*, 1410-1420. https://doi.org/10.1021/cm7024558.

[18] Bagshaw, S. A.; Hayman, A. R. Novel super-microporous silicate templating by ω-hydroxyalkylammonium halide bolaform surfactants. *Chem. Commun.* **2000**, 533-534. https://doi.org/10.1039/B000422G.

[19] Liu, L.; Li, H.; Zhang, Y. Effect of Synthesis Parameters on the Chromium Content and Catalytic Activities of Mesoporous Cr−MSU-*x* Prepared under Acidic Conditions. *J. Phys. Chem. B.* **2006**, *110*, 15478-15485. https://doi.org/10.1021/jp061875o.

[20] Guthrie, C. P.; Reardon, E. J. Metastability of MCM-41 and Al-MCM-41. *J. Phys. Chem. A.* **2008**, *112*, 3386-3390. https://doi.org/10.1021/jp710434y.

[21] Haskouri, J. E.; Cabrera, S.; Caldés, M.; Guillem, C.; Latorre, J.; Beltrán, A.; Beltrán, D.; Marcos, M. D.; Amorós, P. Surfactant-Assisted Synthesis of the SBA-8 Mesoporous Silica by Using Nonrigid Commercial Alkyltrimethyl Ammonium Surfactants. *Chem. Mater.* **2002**, *14*, 2637-2643. https://doi.org/10.1021/cm0116929.

[22] Galarneau, A.; Giscard, D. D.; Renzo, F. D.; Fajula, F. Thermal and mechanical stability of micelle-templated silica supports for catalysis. *Catal. Today* **2001**, *68*, 191-200. https://doi.org/10.1016/S0920-5861(01)00300-5.

[23] Chatterjee, M.; Iwasaki, T.; Hayashi, H.; Onodera, Y.; Ebina, T.; Nagase, T. Characterization of Tetrahedral Vanadium-Containing MCM-41 Molecular Sieves Synthesized at Room Temperature. *Chem. Mater.* **1999**, *11*, 1368-1375. https://doi.org/10.1021/cm981152k.

[24] Mary Thangam, M. A.; Kannan, C. A novel Iron silicate mesoporous material synthesis & its characterization. *Adv. Sci. Lett.* **2018**, *24*, 5532-5536. https://doi.org/10.1166/asl.2018.12143.

[25] Thangam, M. M.; Kannan, C. Isomorphous Substitution of Zn^{2+} in aluminosilicate framework creates two types of mesopores without templates. *Int. J. ChemTech Res.* **2018**, *11*, 365-369. http://dx.doi.org/10.20902/IJCTR.2018.110243.

[26] Kang, F.; Wang, Q.; Xiang, S. Synthesis of mesoporous Al-MCM-41 materials using metakaolin as aluminum source. *Mater. Lett.* **2005**, *59*, 1426-1429. https://doi.org/10.1016/j.matlet.2004.11.057.

[27] Clark, J. H. Catalysis for green chemistry. *Pure Appl. Chem.* **2001**, *73*, 103-111. https://doi.org/10.1351/pac200173010103.

[28] de Zárate, D. O.; Bouyer, F.; Zschiedrich, H.; Kooyman, P. J.; Trens, P.; Iapichella, J.; Durand, R.; Guillem, C.; Prouzet, E. Micromesoporous Monolithic Al-MSU with a Widely Variable Content of Aluminum Leading to Tunable Acidity. *Chem. Mater.* **2008**, *20*, 1410-1420. https://doi.org/10.1021/cm7024558.

[29] Belhakem, A.; Bengueddach, A. Catalytic properties and acidity of modified MCM-41 mesoporous materials with low Si/Al ratio: Heptane isomerisation. *Bull. Chem. Soc. Ethiop.* **2006**, *20*, 99-112. https://doi.org/10.4314/bcse.v20i1.21149.

[30] Kruk, M.; Jaroniec, M.; Kim, J. M.; Ryoo, R. Characterization of highly ordered MCM-41 silicas using X-ray diffraction and nitrogen adsorption. *Langmuir* **1999**, *15*, 5279-5284. https://doi.org/10.1021/la990179v.

[31] Vijayasankar, A. V.; Mahadevaiah, N.; Bhat, Y. S.; Nagaraju, N. Mesoporous aluminophosphate materials: influence of method of preparation and iron loading on textural properties and catalytic activity. *J. Porous Mater.* **2010**, *18*, 369-378. https://doi.org/10.1007/s10934-010-9387-z.

[32] Yu, C.; Fan, J.; Tian, B.; Zhao, D. Morphology Development of Mesoporous Materials: A Colloidal Phase Separation Mechanism. *Chem. Mater.* **2004**, *16*, 889-898. https://doi.org/10.1021/cm035011g.